RESEARCH PAPER

Effect of ambient pressure on the crystalline phase of nano TiO$_2$ particles synthesized by a dc thermal plasma reactor

I. Banerjee · Soumen Karmakar ·
Naveen V. Kulkarni · Ashok B. Nawale ·
V. L. Mathe · A. K. Das · S. V. Bhoraskar

Abstract The synthesis of nanoparticles of titanium dioxide (TiO$_2$) with varying percentages of anatase and rutile phases is reported. This was achieved by controlling the operating pressure in a transferred-arc, direct current thermal plasma reactor in which titanium vapors are evaporated, and then exposed to ambient oxygen. The average particle size remained around 15 nm in each case. The crystalline structure of the as-synthesized nanoparticles of TiO$_2$ was studied with X-ray diffraction analysis; whereas the particle morphology was investigated with the help of transmission electron microscopy. The precursor species responsible for the growth of these nanoparticles was studied with the help of optical emission spectroscopy. As inferred from the X-ray diffraction analysis, the relative abundance of anatase TiO$_2$ was found to be dominant when synthesized at 760 Torr, and the same showed a decreasing trend with decreasing chamber pressure. The study also reveals that anatase TiO$_2$ is a more effective photocatalytic agent in degrading methylene blue by comparison to its rutile phase.

I. Banerjee · S. Karmakar · N. V. Kulkarni ·
A. B. Nawale · V. L. Mathe · S. V. Bhoraskar (✉)
Department of Physics, University of Pune,
Pune 411007, India
e-mail: svb@physics.unipune.ernet.in

A. K. Das
Laser and Plasma Technology Division, Bhabha Atomic
Research Centre, Mumbai 400085, India

Introduction

Titanium dioxide (TiO$_2$) is one of the most widely studied materials, well recognized for its photocatalytic applications, and it has many industrial and research applications (Ollis and Al-Ekabi 1993; Schiavello 1988). An excellent review of its surface properties, which emphasizes the correlation between structure and property, has been presented in exhaustive detail by Diebold (2003). In particular, this author has reviewed the growth mechanisms of different metals as well as metal oxides on TiO$_2$. The review highlights the photoactivity of TiO$_2$ as one of its most interesting and attractive properties (Fujishima and Honda 1972). Experimental and theoretical studies related to the structural and electronic properties of TiO$_2$ (Diebold 2003) are available (Lopez et al. 1992). TiO$_2$ can exist in several stable forms, of which the most abundant ones are anatase, rutile and brookite (Grant 1959; Murray et al. 1993; Samsonov 1982). The energetics of TiO$_2$ polymorphs, with respect to the rutile phase, have been reported (Ranade et al. 2002) and are found to be ∼0.71 kJ/mol lower for brookite and 2.61 kJ/mol higher for the anatase phase. The

brookite phase is stable only at very low temperatures and hence not of great practical importance. The rutile and anatase phases normally co-exist as mixed phases, and efforts are therefore required to obtain a desired pure phase. In recent years, anatase TiO_2 has attracted a great deal of interest because of its technological applications in paints, pigments, and photocatalysis. Anatase TiO_2 has been reported to exhibit higher photocatalytic activity than rutile TiO_2 (Zhou et al. 2002). Much attention is, therefore, focused on preparing anatase TiO_2 with considerably high production rate and size confinement effects, whereas, the mixed phase of anatase (75%) and rutile (25%) is available in the name of P25, which has some commercial importance (Reddy et al. 2002).

The synthesis of TiO_2 on a large scale, with a predetermined crystalline phase, is thus of practical importance. Although chemical routes can produce it in large quantities (Li et al. 2002; Zhou et al. 2002), they mainly result in amorphous structures. It has been well documented (Gao and Zhang 2001) that the amorphous contents in a product of TiO_2 lowers its photocatalytic activity and therefore the synthesis of nanocrystalline TiO_2 is desirable. The results of the chemical routes of synthesis show that the calcination time and temperature have a lot of influence upon nano TiO_2 powder (Li et al. 2002). Although phase transformations of TiO_2 by the calcination process have been studied by many researchers (Li et al. 2002; Haro-Poniatowski et al. 1994) for chemically synthesized TiO_2, reports on the temperatures of reactions vary. It seems that the phase transformations are very dependent upon the process of crystal growth (Diebold 2003). Thus, the problem related to controlling the crystalline phase during the crystal growth of nanoparticles, in addition to large scale production, remains challenging for any given method. Nanocrystalline particles, with sizes typically <10 nm, show higher photocatalytic effects than samples of larger sizes (Gao and Zhang 2001). X-ray absorption spectroscopy was used to identify the local environment of Ti by Wu et al. (2002). Therefore, a detailed study of nanoparticles of TiO_2 has also been an important field of investigation for researchers.

Thermal plasma processes have been proved (Banerjee et al. 2006a, b; Kumar et al. 1999; Padmanabhan et al. 2006) to be effective in producing nanocrystalline materials on account of their high temperature, high enthalpy, and high quenching rate,

thus leading to homogeneous gas-phase condensation. Oh and Ishigaki have used an RF thermal plasma reactor for synthesizing pure rutile and anatase TiO_2 nanoparticles by oxidizing titanium nitride powder (Oh and Ishigaki 2004). The chemical vaporization of TiO_2, induced by a plasma-enhanced ion beam, has been studied by Gracia for the application to optical filters (Gracia et al. 2003). Similarly, the synthesis of nanocrystalline TiO_2 in a plasma reactor has also been reported (Padmanabhan et al. 2006). However, their method requires a feedstock of coarse-grained TiH_2 powder, thereby making the process more complicated than the one used by the authors in the present study.

In her review on TiO_2, Diebold (2003) has stressed the importance of research in the "nanoworld" saying that it provides almost unlimited stimulus for the imagination in terms of how these tiny structures could be used. Diebold has also realized that, in the case of TiO_2, the proven performance improvement of nano-scaled structures in photo-active devices shows a cross fertilization between surface effect and synthesis routes. Thus, keeping in mind the increasing need for different synthesis routes in preparing nanoparticles of TiO_2 on a large scale, we have used the gas-phase condensation method to synthesize TiO_2 with the desired crystalline phase. It is demonstrated that the relative concentrations of the anatase and rutile phases in the as-synthesized, mixed phase of TiO_2 can be controlled by choosing a suitable operating pressure inside the chamber. X-ray diffraction (XRD) analysis is used to characterize crystalline purity. The morphology and size distribution of the as-synthesized nano-phase of TiO_2 have been studied with the help of transmission electron microscopy (TEM). This article also reports the results of photocatalytic degradation of an organic solution, in the presence of the nanoparticles of TiO_2 synthesized under different reactor conditions. The relative merit of the anatase phase in the photocatalytic degradation of methylene blue (MB) has been demonstrated in these mixed-phase, nanocrystalline TiO_2 powders.

Experimental

The oxidation of Ti to form TiO_2 is highly exothermic. The enthalpy of formation of TiO_2 is -944.74 kJ mol^{-1} (Barin and Platzki 1995). Keeping

this fact in mind in the present experiment, TiO_2 was synthesized by the process of thermal plasma-assisted, gas-phase condensation involving homogeneous nucleation. The schematic of the plasma reactor used in the present experiment is shown in Fig. 1. Plasma was generated by a dc transferred arc process using a torch mounted on the upper flange of the cylindrical retort, which allows for vertical movement over a length of 300 mm. The cathode was made up of thoriated tungsten with a 6-mm diameter, and was mounted on the water cooled copper base. An auxiliary anode in the form of a nozzle was used for starting the pilot arc, which helped in stabilizing the plasma jet. The jet was subsequently transferred to the anode, which in the present case was made up of a 99.00% pure titanium block placed on the graphite container. The graphite anode was held on a water cooled copper target equipped with a movable shaft, and was fitted on the bottom flange.

The reactor chamber was 35 cm, in diameter and 60 cm in height, and was covered at both ends by double walled stainless steel flanges. Two ports, one for viewing the arc column during the evaporation of metal and the other to enable optical emission spectroscopic (OES) measurements, were provided. The plasma temperature was determined by using the atomic Boltzmann plot method (Banerjee et al. 2006a, b; Joshi et al. 1997).

The plasma-forming gas was argon, which was made to flow at a rate of 5 lpm through the plasma torch. The torch was operated by 10 kW DC power at 100 A. The reacting gas was oxygen, the flow rate of which was maintained at 10 lpm. It was purged into the reactor in such a way as to form a uniform envelope around the plasma plume. Argon plasma from the torch was allowed to impinge on the metal anode and subsequently transfer its heat to the titanium target. The anode was evaporated and was allowed to react with the surrounding oxygen. The reactor was pre-evacuated to a base pressure of $\sim 10^{-3}$ Torr. During the synthesis, the throttle valve was adjusted to achieve the desired pressure in the reactor, varying from 760 to 100 Torr in the series of experiments. The reaction products were collected over the substrates mounted on the hemispherical stainless steel water-cooled collector, housed at a radial distance of 12 cm from the anode substrate. This hemispherical collector allowed the particles to travel an equal distance before they were deposited. Table 1 describes the operating parameters of the reactor during the synthesis.

In situ recordings of the emission spectra were carried out with a Jobin Yvon Spex 270 M spectrometer, fitted with a grating of 1,200 lines/cm and blazed in the visible region (540 nm). The detector was a thermo electric cooled, front illuminated CCD, with a $256 \times 1,024$ pixel array made up of 26 micron

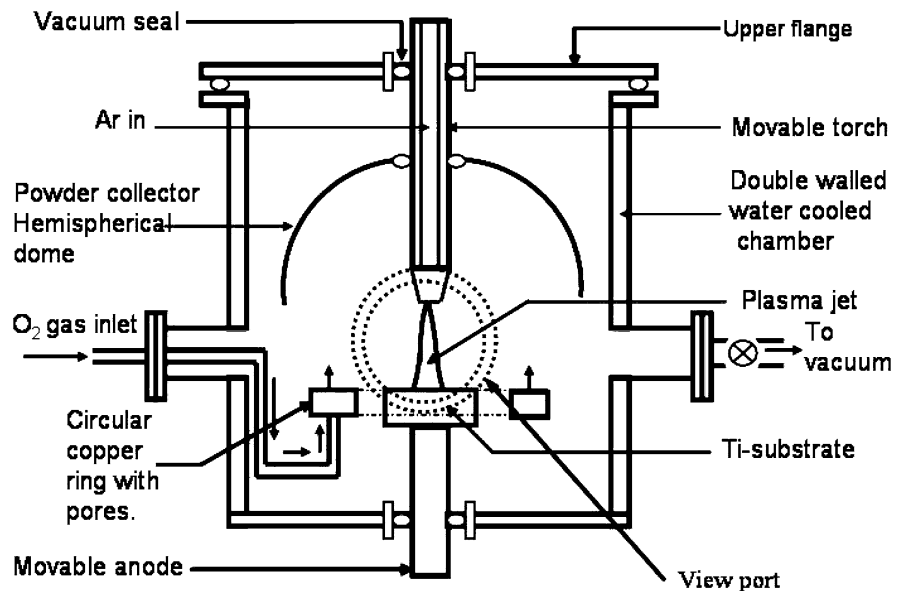**Fig. 1** Schematic diagram of the thermal plasma reactor used for the synthesis of nano TiO_2 particles

Vacuum seal
Upper flange
Ar in
Movable torch
Powder collector Hemispherical dome
Double walled water cooled chamber
O_2 gas inlet
Plasma jet
To vacuum
Circular copper ring with pores.
Ti-substrate
Movable anode
View port

Table 1 Operating parameters of the reactor during the synthesis of TiO$_2$

S. No.	Physical parameter	Operating regime
1.	Arc current (A)	100
2.	Voltage (V)	100
3.	DC power (kW)	10
4.	Water flow rates to:	
	(a) Cathode (LPM)	8
	(b) Substrate (LPM)	10
	(c) Nozzle (LPM)	10
	(d) Chamber walls (LPM)	22
	(e) Top flange and powder collection zone (LPM)	12
5.	Gas flow rates:	
	(a) Plasma forming gas (argon) (LPM)	5
	(b) Ambient gas (oxygen) (LPM)	10
6.	Base pressure (Torr)	10^{-3}
7.	Operating pressure (Torr)	100, 300, 500, and 760

square pixels, resulting in a total detector dimension of 26.6 × 6.6 mm. The linear dispersion of the spectrometer was 3.1 nm/mm, offering a spectral resolution of ≤0.1 nm when coupled with the CCD. Further details of the analysis of emission spectra are described in our earlier communication (Banerjee et al. 2006a, b).

The collected powder was characterized with a Phillips X-ray diffractometer (Model PW-1840) and a JEOL 1200 EXTEM. For this analysis, the as-synthesized powder sample was sonicated in isopropyl alcohol for 30 min, and a small drop was spread on the carbon-coated copper grid for analysis by TEM.

Photocatalytic degradation was monitored by recording the photo-absorption peak at 640 nm for the organic stain reagent, MB, after adding the as-synthesized TiO$_2$ powder and irradiating by UV radiation for a known duration. The buffer solution was prepared by dissolving 1 mg of MB in 100 mL of distilled water. The absorption level was optimized for 7.2 mg of TiO$_2$ in the buffer solution.

Results and discussion

Synthesis of nano TiO$_2$ particles

Before analyzing the characteristic properties of the as-synthesized TiO$_2$, the rate of production in the thermal plasma reactor was determined by measuring the weight loss of the anode material, followed by the measurements of the weights of the collected nanoparticles synthesized at different ambient pressures of the reactor. These weights are shown in Table 2 for four different ambient pressures ranging from 760 to 100 Torr. The results indicate that the rate of production of the as-synthesized TiO$_2$, within the experimental limits of accuracy, decreases as the operating pressure decreases.

he efficiency of the reactor in terms of the anode material consumed vis-à-vis the total production of nanoparticles was observed to be around 60% by weight. After the growth, the nano-particles fly from the plasma zone in all directions and get deposited on the walls of the reactor. The particles deposited on the hemispherical dome were collected for further characterization. The oxide nanoparticles were found to be non-agglomerated. The distribution by weight of nano-particles collected in different parts of the reactor was approximately (i) 40% over the hemispherical collector, (ii) 10% over the body of the

Table 2 Rate of production of TiO$_2$ during the synthesis

S. No.	Ambient pressure (Torr)	TiO$_2$ (g/h) ± 10%
1.	760	25
2.	500	12
3.	300	8
4.	100	4

torch, (iii) 30% on the walls of the cylindrical chamber, and (iv) around 20% over the other parts of the reactor.

Characteristics of the synthesized nano TiO_2 particles

The powder collected from the reactor was subjected to structural characterization by XRD analysis. The most intense lines found from the JCPDS data, corresponding to the (101) plane of anatase TiO_2, occur at $2\theta = 25.3°$, whereas a similar peak arising from the (110) plane of rutile TiO_2 occurs at $2\theta = 27.4°$ (where θ is the diffraction angle). Relative concentrations of the two crystalline phases were estimated using the intensities of the above two XRD lines. Figure 2 shows the XRD pattern for values of 2θ ranging from 20° to 30°. The amplitudes of the two peaks ('A' for anatase and 'R' for rutile TiO_2) have been shown together for the four samples synthesized at operating pressures of 760, 500, 300 and 100 Torr. It is very interesting to note that the relative intensities differ systematically for these samples. The amplitude of the peak 'A' shows a decrease with decreasing operating pressure, whereas the amplitude of the peak 'R' shows an opposite trend. The relative intensity ratio defined as F = amplitude of 'A'/amplitude of 'R' is then plotted in Fig. 3 to illustrate the abundance of one phase relative to the other.

A steady increase in F, from 0.7 to 2.4, indicates that the ambient pressure during the synthesis exerts a strong control over the crystalline phases. From Fig. 2a we can also see that a high operating pressure helps in the formation of anatase, whereas a decrease in this pressure favors the growth of the rutile phase.

The change in the crystalline phase, based on the operating pressure in the reactor, can be explained by the cluster chemistry of the vapor phase condensation. The process starts with the evaporation of the anode (titanium in the present case) due to plasma interaction. The resulting vapors fill the space above the anode surface and diffuse out into the plasma zone, followed by chemical reactions with oxygen, which diffuses inside the plasma column and surrounds it. Figure 4a illustrates this process conceptually. As a result of this reaction, molecular species are formed inside the plasma region. The presence of Ti–O species is, in fact, confirmed by the
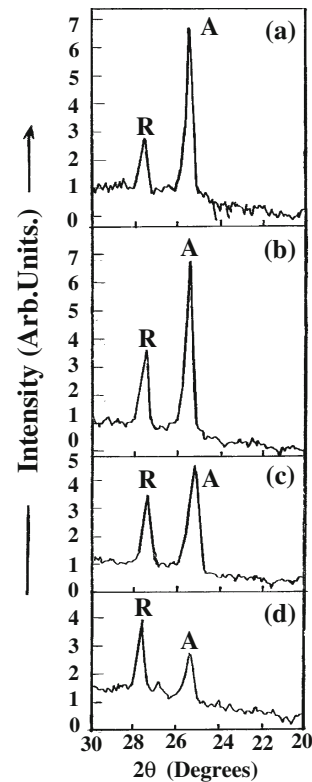

Fig. 2 XRD pattern showing the major lines of anatase 'A' ($2\theta = 25.30$, $d = 3.52$, *hkl*: 101) and rutile 'R' ($2\theta = 27.43$, $d = 3.25$, *hkl*: 110) phase of the TiO_2 nano particles at **a** 760 Torr, **b** 500 Torr, **c** 300 Torr, and **d** 100 Torr
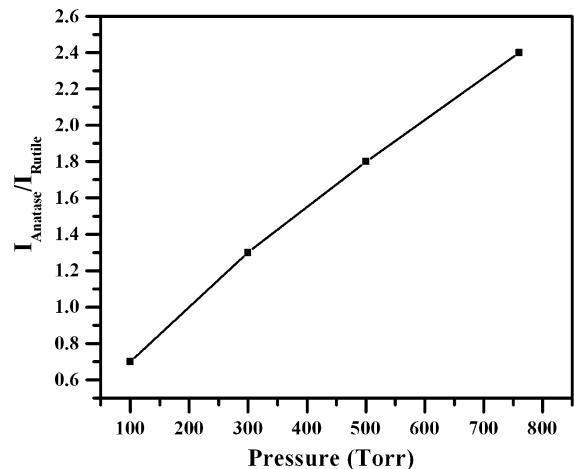

Fig. 3 The plot showing the ratios of the peak intensities of major lines of anatase and rutile phases determined from the corresponding XRD patterns (Fig. 2) as a function of the operating pressure

emission spectrum, a typical plot of which is shown in Fig. 4b. The spectrum shows the fine structure of the Ti–O bands, with lines appearing at 665.1, 668.1, 671.9, 685.2, 671.9, 685.2, 705.4, 712.5, 719.7, 721.9, and 726.9 nm. The wavelengths have been compared with the reported values of emission lines arising from Ti–O species (Pearse and Gaydon 1976). These spectral lines provide evidence for the presence of Ti–O species inside the plasma. Subsequently, these species diffuse out of the hot plasma and then aggregate to form the nucleation sites just outside the boundaries of the plasma plume.

It seems that the crystalline phase of the embryos is decided by two factors: (a) the available oxygen for growth and (b) the extent of supercooling during their formation. As the ambient operating pressure is reduced in the chamber, the partial pressure of oxygen also decreases. The lower oxygen content favors the growth of the rutile phase during the synthesis of TiO_2 from titanium nitride by controlling the oxygen flow in the RF thermal plasma reactor, as has been very clearly demonstrated by Oh and Ishigaki (2004). They observed the characteristic Raman bands of the rutile TiO_2 at 147, 236, 447, and 611 cm^{-1} in the powders synthesized under low oxygen flow rates. The synthesis of nanoparticles with an abundance of rutile structure is very important since the review (Diebold 2003) states that nanostructures of TiO_2 are almost either amorphous or of anatase form. Moreover, it is agreed that there might be a clear connection between the surface properties and the synthesis routes.

The later assumption about enhanced supercooling arises from our observations of the expanded plasma plume near the substrate as the pressure is decreased. Due to sub-atmospheric pressures, the plasma near the boundaries starts deviating from the local conditions of thermodynamic equilibrium. As a result, the temperature associated with the plasma plume also decreases. Therefore, the nucleation occurring at the plasma boundary under such conditions seems to favor the formation of the defective, oxygen-deficient rutile phase of TiO_2. The high temperature, vapor-phase condensation, as in the present case, results from homogeneous nucleation.

The morphology of the as-synthesized TiO_2 was studied by TEM. A typical TEM micrograph is shown in Fig. 5a. Figure 5b shows that spherical particles of size 10 nm are the most abundant. To get information about the crystallinity of such a single particle, the selected area electron diffraction (SAED) pattern was recorded, and is shown in Fig. 5c. The pattern shows spots as well as faint rings, which are characteristic of nanomaterials. The Miller indices that correspond to anatase and rutile TiO_2 are indicated on the diffraction pattern shown in Fig. 5c. It is clearly evident that the nanoparticles are highly crystalline and this agrees well with the results obtained by XRD analysis. TEM micrographs and SEAD patterns were not very different for the four samples, and therefore a typical micrograph is shown in Fig. 5. The surface area analysis of the as-synthesized TiO_2 was done by using the BET single point technique. The average was determined to be ~30 m^2/g for all the products. By using the experimentally determined surface area and assuming that all particles are spherical, the average particle size (d_{BET}) was calculated for the as-synthesized particles as follows:

Fig. 4 a Schematic of plasma plume showing the species of titanium and oxygen to form titanium oxide precursors. b Optical Emission Spectra (OES) recorded during the synthesis of titanium oxide indicating the presence of Ti–O molecular bands
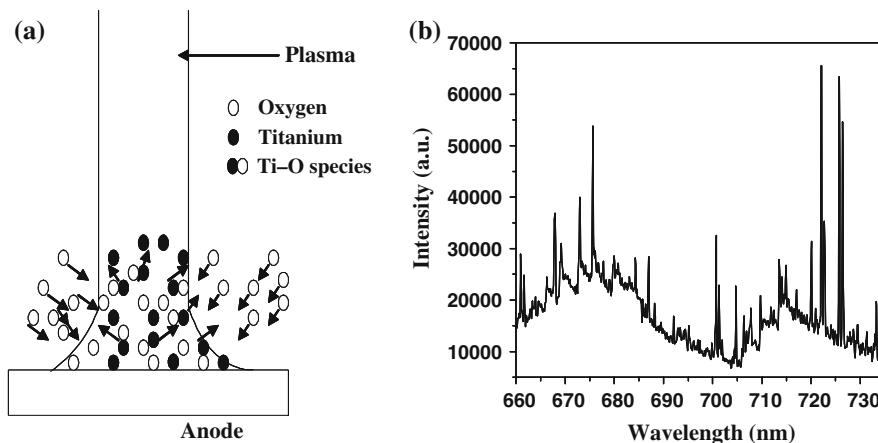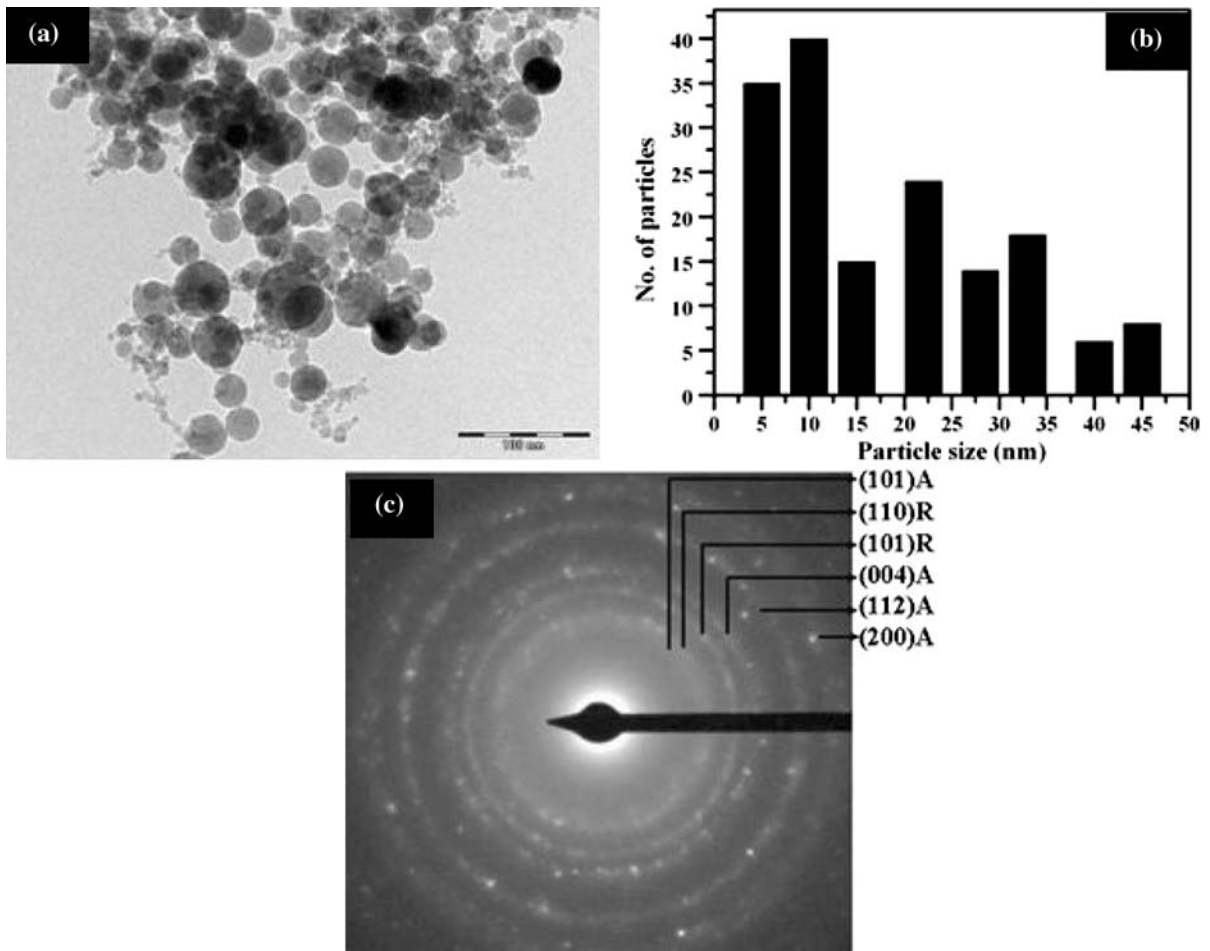
Fig. 5 **a** A typical TEM micrograph of the nano TiO_2 particles synthesized at 760 Torr of ambient pressure, **b** particle size distribution, **c** selected area electron diffraction (SAED) pattern of the nano TiO_2 particles synthesized at 760 Torr of ambient pressure

$$d_{BET} = 6/\rho S_v \qquad (1)$$

where ρ is the material's density and S_v the specific surface area of the sample. By using the theoretical density of 4 g/cm^3 for TiO_2, the calculated d_{BET} for the as-synthesized TiO_2 powder was 5 nm, which approximates the TEM data.

Photocatalytic degradation studies

Figure 6a, b shows the absorption spectra of MB, with and without TiO_2 (synthesized at 760 Torr), after irradiation by a UV source at different intervals of time. The percent residual concentration of the MB solution after addition of nano TiO_2 powder irradiated by UV light has been plotted in Fig. 6c as a

function of the time elapsed. Figure 7a shows the absorption spectra plotted for different samples synthesized at different ambient pressures. The samples were irradiated by UV for 150 min. The amount of degradation is seen to increase consistently as the operating chamber pressure was increased from 100 to 760 Torr. The reduction in the absorbance level for this extreme condition is estimated to be $\sim$75% (Fig. 7b). These results can be correlated to the structural phases of the samples. It has been noticed that the sample synthesized at 760 Torr is predominantly anatase in phase, whereas that synthesized at 100 Torr is of rutile phase. The fact that the specimen synthesized at 760 Torr shows the maximum degradation is in accordance with the literature (Matunaga et al. 1985). The photocatalytic
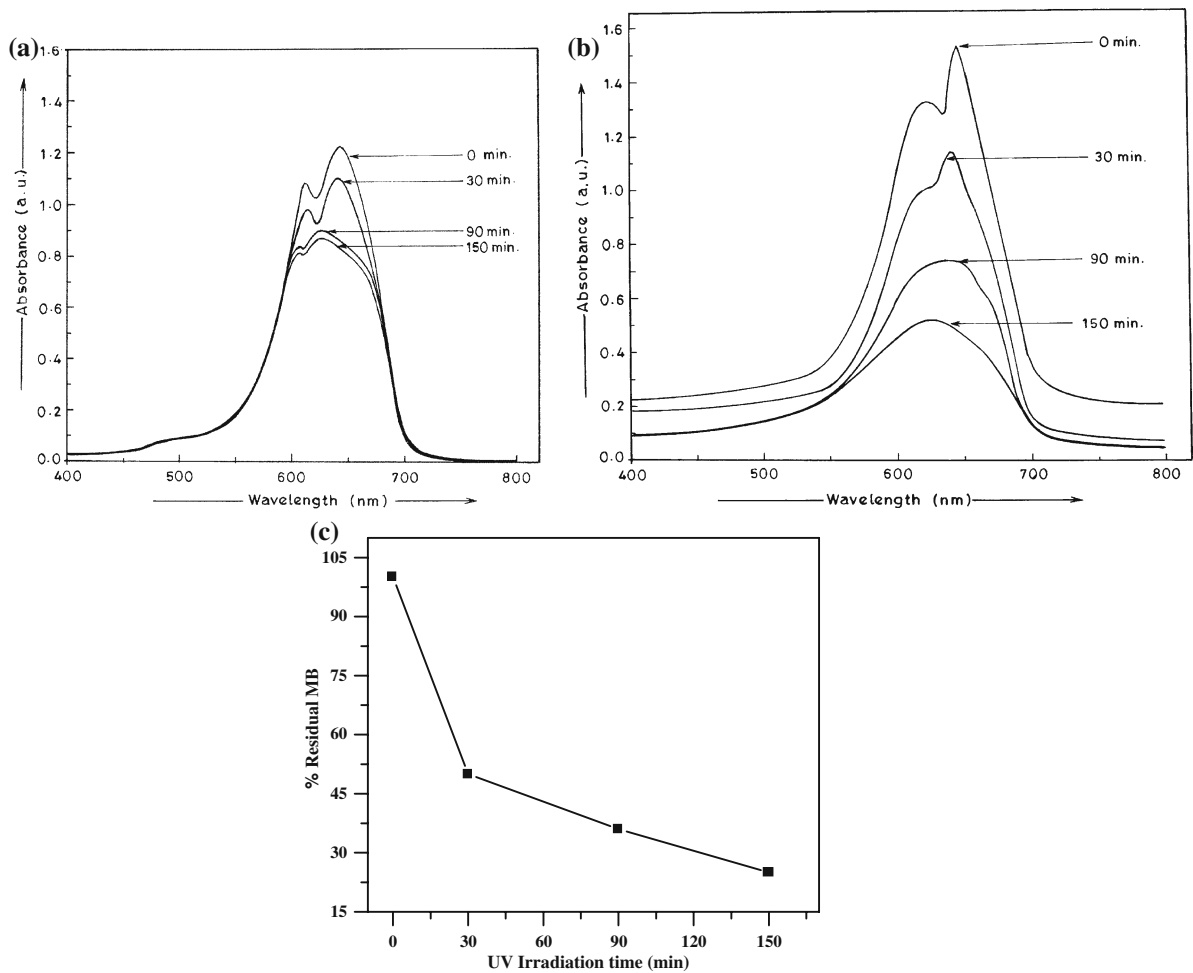
Fig. 6 a Absorbance characteristics of methylene blue at different time intervals on UV irradiation, **b** absorbance characteristics of methylene blue added with nano TiO$_2$ particles at different time intervals on UV irradiation, and **c** residual concentration of methylene blue added with nano TiO$_2$ after UV irradiation for different time intervals

activity of anatase TiO$_2$ has been well established (Huang et al. 2000; Fujishima et al. 2000) and it is known to exhibit better degradation of organic reagents as compared to the rutile phase. A similar study for the thermal plasma-synthesized, nanostructured TiO$_2$ is reported by Padmanabhan et al. (2006). The results obtained for the residual concentration of MB may be due to the broad particle size distribution in the present study. The photocatalytic degradation of MB was carried out under UV radiation in the presence of the as-synthesized nano TiO$_2$ particles. The degradation of MB was monitored at different time intervals using a UV–visible absorption spectrophotometer.

Conclusions

This article reports the influence of the operating pressure in a dc arc thermal plasma reactor on the crystalline phase of TiO$_2$. The relative abundances of the anatase and rutile phases were seen to be affected by the operating pressure. The anatase phase was found to be prominent at 760 Torr, whereas the rutile phase was the major phase at 100 Torr. Moreover, the variation of the ratio of the relative concentration of anatase to that of rutile was found to increase linearly with an increase in the operating chamber pressure. The crystalline phase formation of the as-synthesized TiO$_2$ is explained on the basis of the different oxygen
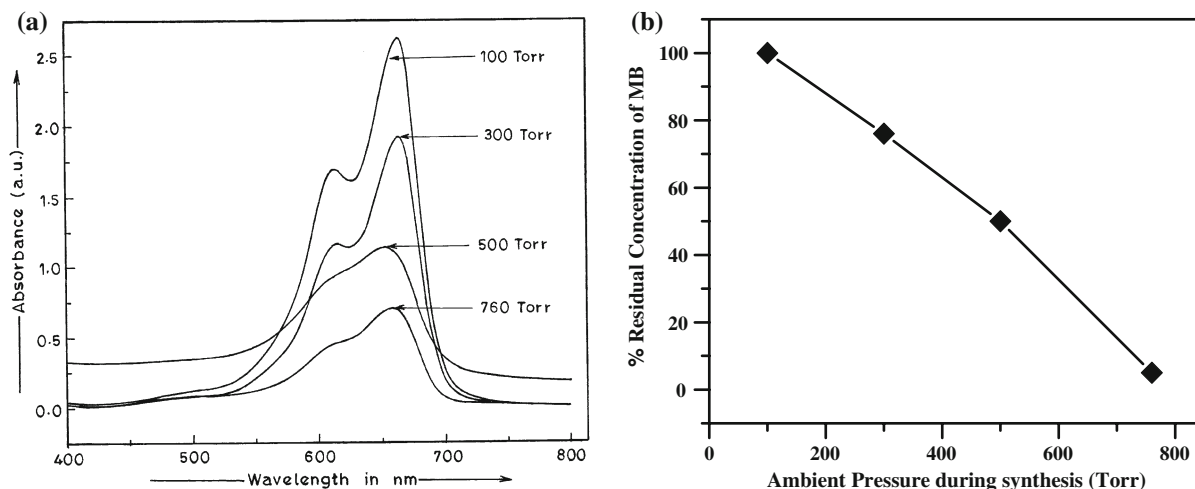
Fig. 7 **a** Absorbance characteristics of methylene blue added with nano TiO$_2$ particles synthesized at different ambient pressure on UV irradiation and **b** residual concentration of methylene blue added with nano TiO$_2$ synthesized at different ambient pressure after UV irradiation for 150 min

content available at different operating pressures. The formation of oxygen-deficient rutile clusters is favored by enhanced supercooling, and they act as nucleating sites for further growth. Results from in situ optical emission spectroscopy reveal that the molecular species of Ti–O were generated inside the plasma plume during the synthesis of TiO$_2$, and they were the species responsible for the growth of different crystalline phases of the as-synthesized TiO$_2$. A detailed analysis of the reaction products was carried out with the help of XRD and TEM investigations. The strategically important anatase phase is shown to exhibit superior photocatalytic activity during the degradation of methylene blue.

References

Banerjee I, Joshi NK, Sahasrabudhe SN, Kulkarni NV, Karmakar S, Pasricha R, Ghorui S, Tak AK, Murthy PSS, Bhoraskar SV, Das AK (2006a) In situ optical emission spectroscopic investigations during arc plasma synthesis of iron oxide nanoparticles by thermal plasma. IEEE Trans Plasma Sci 34:1175–1182. doi:10.1109/TPS.2006.878430

Banerjee I, Joshi NK, Sahasrabudhe SN, Karmakar S, Kulkarni NV, Ghorui S, Tak AK, Murthy PSS, Bhoraskar SV, Das AK (2006b) In situ studies of emission characteristics of the DC arc thermal plasma column during synthesis of nano-AlN particles. IEEE Trans Plasma Sci 34:2611–2617. doi:10.1109/TPS.2006.886059

Barin I, Platzki G (1995) Thermochemical data of pure substances. VCH Publishers, Wienheim

Diebold U (2003) The surface science of titanium dioxide. Surf Sci Rep 48:53–229. doi:10.1016/S0167-5729(02)00100-0

Fujishima A, Honda K (1972) Electrochemical photolysis of water at a semiconductor electrode. Nature 238:37–38. doi:10.1038/238037a0

Fujishima A, Rao TN, Donald A, Tryk J (2000) Titanium dioxide photocatalysis. J Photochem Photobiol Chem 1:1–21. doi:10.1016/S1389-5567(00)00002-2

Gao L, Zhang Q (2001) Effect of amorphous contents and particle size on photocatalytic properties of TiO$_2$ nanoparticles. Scr Mater 44:1195–1198. doi:10.1016/S1359-6462(01)00681-9

Gracia F, Holgado JP, Contreras L, Girardeau T, González-Elipe AR (2003) Optical and crystallisation behaviour of TiO$_2$ and V/TiO$_2$ thin films prepared by plasma and ion beam assisted methods. Thin Solid Films 429:84–90. doi:10.1016/S0040-6090(03)00431-0

Grant FA (1959) Properties of rutile (titanium dioxide). Rev Mod Phys 31:646–674. doi:10.1103/RevModPhys.31.646

Haro-Poniatowski E, Rodríguez-Talavera R, de la Cruz Heredia M, Cano-Corona O, Arroyo-Murillo R (1994) Crystallization of nanosized titania particles prepared by the sol–gel process. J Mater Res 9:2102–2108. doi:10.1557/JMR.1994.2102

Huang Z, Maness C, Blake DM, Wolfrum EJ, Smolinski SL, Jocoby WA (2000) Bactericidal mode of titanium dioxide

photo-catalysis. J Photochem Photobiol A 130:163–170. doi:10.1016/S1010-6030(99)00205-1

Joshi NK, Sahasrabudhe SN, Sreekumar KP, Venkatramani N (1997) Variation of axial temperature in thermal plasma jets. Meas Sci Technol 8:1146–1150. doi:10.1088/0957-0233/8/10/016

Kumar PM, Balasubramanian C, Sali ND, Bhoraskar SV, Rohatgi VK, Badrinarayanan S (1999) Nano phase alumina synthesis in thermal arc plasma and characterization: correlation to the gas phase studies. Mater Sci Eng B Solid 63:215–227. doi:10.1016/S0921-5107(99)00038-0

Li B, Wang X, Yan M, Li L (2002) Preparation and characterization of nano TiO_2 powder. Mater Chem Phys 78:184–188. doi:10.1016/S0254-0584(02)00226-2

Lopez T, Sanchez E, Bosch P, Meas Y, Gomez R (1992) FTIR and UV-vis (diffuse reflectance) spectroscopic characterization of TiO_2 sol-gel. Mater Chem Phys 32:141–152

Matunaga T, Tomoda R, Nakajima T, Wake H (1985) Photo-electro-chemical sterilization of microbial cells by semiconductor powders. FEMS Microbiol Lett 29:211–214. doi:10.1111/j.1574-6968.1985.tb00864.x

Murray CB, Norris DJ, Bawendi MG (1993) Synthesis and characterization of nearly monodisperse CdE (E = sulfur, selenium, tellurium) semiconductor nanocrystallites. J Am Chem Soc 115:8706–8715. doi:10.1021/ja00072a025

Oh S, Ishigaki T (2004) Preparation of the pure rutile and anatase TiO_2 nanopowders using RF thermal plasma. Thin Solid Films 457:186–191. doi:10.1016/j.tsf.2003.12.043

Ollis DF, Al-Ekabi H (1993) Photocatalytic purification and treatment of water and air. Elsevier, Amsterdam

Padmanabhan PVA, Sreekumar KP, Thiyagarajan TK, Satpute RU, Bhanumurthy K, Sengupta P, Dey GK, Warrier KGK (2006) Nanocrystalline titanium dioxide formed by reactive plasma synthesis. Vacuum 80:1252–1255. doi:10.1016/j.vacuum.2006.01.054

Pearse RWB, Gaydon AG (1976) The identification of molecular spectra, 2nd edn. Chapman & Hall, London

Ranade MR, Navrotsky A, Zhang HZ, Banfield JF, Elder SH, Zaban A, Borse PH, Kulkarni SK, Doran GS, Whitfield HJ (2002) Energetics of nanocrystalline TiO_2. Proc Natl Acad Sci USA 99:6476–6481. doi:10.1073/pnas.251534898

Reddy KM, Manorama SV, Reddy AR (2002) Bandgap studies on anatase titanium dioxide nanoparticles. Mater Chem Phys 78:239–245. doi:10.1016/S0254-0584(02)00343-7

Samsonov GV (1982) The oxide handbook. IFI/Plenum Press, New York

Schiavello M (1988) Photocatalysis and environment trends and applications. NATO ASI series. Kluwer Academic Publishers, Dordrecht

Wu ZY et al (2002) Structural determination of Titanium-dioxide nanoparticles by X-ray absorption spectroscopy. Appl Phys Lett 80:2973–2975

Zhou XF, Chu DB, Wang SW, Lin CJ, Tian ZQ (2002) New routes to prepare nanocrystalline TiO_2 and its reaction mechanism. Mater Res Bull 37:1851–1857. doi:10.1016/S0025-5408(02)00863-2